Memoirs of the Faculty of Engineering, Okayama University, Vol.26, No. 2, pp.139-150, March 1992

Scattering by a Penny-Shaped Crack Subject to Oblique Incident Waves

Sohichi HIROSE*

(Received January 12 , 1992)

SYNOPSIS

Scattering problems by a penny-shaped crack are solved using a time-domain boundary integral equation method. The crack is located in an infinite homogeneous, isotropic, linearly elastic solid, and is subjected to an oblique incident wave of either P-, SV-, or SH-wave. The hypersingular integral equation is solved to obtain near-field solutions as well as scattered far-fields. The accuracy of the present method is confirmed by comparing the near-field solutions for different arrangement of elements. Scattered far-fields are calculated for various incident waves, and their usefulness in quantitative non-destructive evaluation is discussed.

1. INTRODUCTION

In application of fracture mechanics to the evaluation of material strength and service life of the structure, it is no good enough just to detect a flaw or the presence of interior material properties. Detailed information about a defect such as its location, shape, orientation, size and material properties is required. Of recent concern in non-destructive evaluation is, therefore, to determine such quantitative values from observed experimental data. This procedure is called quantitative non-destructive evaluation (QNDE). A more rigorous and fundamental approach plays an important role in QNDE. For example, the scattering theory in elastodynamics can give basic equations for quantitative ultrasonic techniques. Stress waves, which penetrate a material and are scattered by a defect, may be understood quantitatively in terms of the scattering theory. This paper will consider scattering problems by a penny-shaped crack, which may give some information for determining geometrical parameters of the crack. The scattering problem itself is a forward problem, for which geometry and material property of a defect are given beforehand. The solution may, however, provide useful information for the inverse problem of characterizing the defect.

The dynamic fields generated by the interaction of elastic waves with a penny-shaped crack have usually been analyzed in the frequency domain. Semi-analytical methods in the frequency domain

* Department of Civil Engineering

have been fairly well reviewed by Martin and Wickham[7]. Numerical approaches have also been used for frequency-domain scattering problems by Lin and Keer[6], Budreck and Achenbach[1] and Nishimura and Kobayashi[8]. It is, of course, possible to use frequency-domain results in conjunction with the fast Fourier transform technique to construct time-domain results. There are, on the other hand, very few studies on the direct approach towards the time-domain solution to 3-D crack scattering problems. Hirose and Achenbach[2,3,4] have solved several scattering problems from penny-shaped and elliptical cracks subjected to a normally incident wave, using a time-domain boundary integral equation method. This paper will be concerned with further application of the time-domain boundary integral equation method to scattering of obliquely incident waves by a penny-shaped crack. Attention is focused on the scattered far-fields, which may be useful for determining the orientation of a crack.

2. FORMULATION OF BOUNDARY INTEGRAL EQUATION[4,5]

We consider the scattering of elastic waves by a crack S included in a three-dimensional infinite domain D, which is occupied by a homogeneous, isotropic, linearly elastic solid. For the scattering problem, the total field $\boldsymbol{u}$ in D may be written as the sum of the incident and scattered fields

$$\boldsymbol{u}(\boldsymbol{x},t) = \boldsymbol{u}^{in}(\boldsymbol{x},t) + \boldsymbol{u}^{sc}(\boldsymbol{x},t). \tag{1}$$

The components of the displacement vector $\boldsymbol{u}$ are governed by

$$C_{ijkl}u_{k,lj} = \rho\ddot{u}_i, \tag{2}$$

where ρ is the mass density and a dot stands for differentiation with respect to time t, and

$$C_{ijkl} = \lambda\delta_{ij}\delta_{kl} + \mu(\delta_{ik}\delta_{jl} + \delta_{il}\delta_{jk}) \quad (\ \lambda,\ \mu\text{: Lamé constants }). \tag{3}$$

Eq.(2) must be supplemented by appropriate initial and boundary conditions.

The solution $\boldsymbol{u}$ of eq.(2) is subject to the initial condition.

$$\boldsymbol{u}(\boldsymbol{x},0) = \boldsymbol{u}^{in}(\boldsymbol{x},0) \quad \text{in } D. \tag{4}$$

The boundary conditions on the crack faces are given by

$$\begin{aligned} t_i^{\pm}(\boldsymbol{x},t) &\equiv C_{ijkl}u_{k,l}^{\pm}(\boldsymbol{x},t)n_j(\boldsymbol{x}) \\ &= 0 \quad \text{in } S\times[0,\infty). \end{aligned} \tag{5}$$

Here $\pm$ indicates the limit from the positive (negative) side of the coordinate normal to S, and $\boldsymbol{n}$ is a normal vector from the negative side to the positive one of S. The scattered field $\boldsymbol{u}^{sc}$ satisfies the following radiation condition

$$\begin{aligned} &\lim_{|\boldsymbol{x}|\to\infty}|\boldsymbol{x}|\left(\frac{\partial\boldsymbol{u}^{sc(L)}}{\partial|\boldsymbol{x}|}+\frac{1}{c_L}\frac{\partial\boldsymbol{u}^{sc(L)}}{\partial t}\right)=\boldsymbol{0}, \qquad \lim_{|\boldsymbol{x}|\to\infty}\boldsymbol{u}^{sc(L)}=\boldsymbol{0}, \\ &\lim_{|\boldsymbol{x}|\to\infty}|\boldsymbol{x}|\left(\frac{\partial\boldsymbol{u}^{sc(T)}}{\partial|\boldsymbol{x}|}+\frac{1}{c_T}\frac{\partial\boldsymbol{u}^{sc(T)}}{\partial t}\right)=\boldsymbol{0}, \qquad \lim_{|\boldsymbol{x}|\to\infty}\boldsymbol{u}^{sc(T)}=\boldsymbol{0}, \end{aligned} \tag{6}$$

uniformly for all directions $\boldsymbol{x}$. Here $\boldsymbol{u}^{sc(L)}$ and $\boldsymbol{u}^{sc(T)}$ are the lamellar and solenoidal parts of the scattered field, respectively, and c_L and c_T are the velocities of longitudinal and transverse waves, respectively.

The solution $\boldsymbol{u}$ of eq.(2) may be written in the following integral form:

$$\begin{aligned} u_k(\boldsymbol{x},t) &= u_k^{in}(\boldsymbol{x},t) - \int_S U_{ik}(\boldsymbol{y},t;\boldsymbol{x}) * \{t_i^+(\boldsymbol{y},t) - t_i^-(\boldsymbol{y},t)\} dS_y \\ &+ \int_S T_{ik}(\boldsymbol{y},t;\boldsymbol{x}) * \{u_i^+(\boldsymbol{y},t) - u_i^-(\boldsymbol{y},t)\} dS_y \quad \boldsymbol{x} \in D, \end{aligned} \tag{7}$$

where the asterisk denotes the convolution integral with respect to time. In eq.(7), $\boldsymbol{U}$ and $\boldsymbol{T}$ are fundamental solutions for a three-dimensional transient elastodynamic problem, given by

$$\begin{aligned} U_{ik}(\boldsymbol{y},t;\boldsymbol{x}) &= \frac{1}{4\pi\rho r}\left\{(3r_{,i}r_{,k} - \delta_{ik})\int_{c_L^{-1}}^{c_T^{-1}} \lambda\delta(t-\lambda r)d\lambda \right. \\ &\left. + r_{,i}r_{,k}\left[\frac{1}{c_L^2}\delta(t-\frac{r}{c_L}) - \frac{1}{c_T^2}\delta(t-\frac{r}{c_T})\right] + \frac{\delta_{ik}}{c_T^2}\delta(t-\frac{r}{c_T})\right\}, \end{aligned} \tag{8}$$

$$T_{ik}(\boldsymbol{y},t;\boldsymbol{x}) = C_{ijpq}\frac{\partial}{\partial y_q}U_{pk}(\boldsymbol{y},t;\boldsymbol{x})n_j(\boldsymbol{y}), \tag{9}$$

where $r = |\boldsymbol{x} - \boldsymbol{y}|$ and $\delta(\cdot)$ is the Dirac delta function.

Applying the traction operator $C_{jpkq}n_p(\boldsymbol{x})\partial/\partial x_q$ to eq.(7), we obtain the integral representation of the traction

$$\begin{aligned} t_j(\boldsymbol{x},t) &= t_j^{in}(\boldsymbol{x},t) - \int_S V_{ij}(\boldsymbol{y},t;\boldsymbol{x}) * \{t_i^+(\boldsymbol{y},t) - t_i^-(\boldsymbol{y},t)\} dS_y \\ &+ \int_S W_{ij}(\boldsymbol{y},t;\boldsymbol{x}) * \{u_i^+(\boldsymbol{y},t) - u_i^-(\boldsymbol{y},t)\} dS_y \quad \boldsymbol{x} \in D, \end{aligned} \tag{10}$$

where $V_{ij}(\boldsymbol{y},t;\boldsymbol{x})=C_{jpkq}n_p(\boldsymbol{x})\partial U_{ik}(\boldsymbol{y},t;\boldsymbol{x})/\partial x_q$ and $W_{ij}(\boldsymbol{y},t;\boldsymbol{x})=C_{jpkq}n_p(\boldsymbol{x})\partial T_{ik}(\boldsymbol{y},t;\boldsymbol{x})/\partial x_q$.

Considering the boundary condition of eq.(5) and taking the limit $\boldsymbol{x} \in D \to \boldsymbol{X} \in S$ in eq.(10), we have the boundary integral equation for a crack as follows:

$$-t_j^{in}(\boldsymbol{X},t) = p.f.\int_S W_{ij}(\boldsymbol{y},t;\boldsymbol{X}) * [u_i(\boldsymbol{y},t)] dS_y \quad \boldsymbol{X} \in S, \tag{11}$$

where $p.f.$ denotes the finite part of the integral and $[\boldsymbol{u}]$ indicates the crack-opening displacement defined as $[\boldsymbol{u}] = \boldsymbol{u}^+ - \boldsymbol{u}^-$.

3. NUMERICAL IMPLEMENTATION

Since it is difficult to obtain solutions of eq.(11) in a closed form, the integral equation (11) has to be solved numerically in conjunction with the boundary element technique. In this paper, the unknown crack-opening displacement $[\boldsymbol{u}]$ is represented by piecewise linear functions in time and by the crack-opening displacement for the corresponding static problem for the spatial distribution. The time axis is discretized into a sequence of small increments Δt. Also the crack face S is divided into Q quadrilateral elements, i.e., $S = \sum_{q=1}^{Q} S_q$. The centroid on each element is taken as a collocation point. The unknown $[\boldsymbol{u}]$ is then expressed by

$$[u_i(\boldsymbol{y},t)] = \sum_{q=1}^{Q} \psi_q(\boldsymbol{y}) \sum_m \eta^m(t)[u_i]_q^m \tag{12}$$

where $\psi_q(\boldsymbol{y})$ denotes the spatial shape function related to the q-th node, and $\eta^m(t)$ is the interpolation function in time defined as

$$\eta^m(t) = \bar{\eta}^{m-1}(t) - 2\bar{\eta}^m(t) + \bar{\eta}^{m+1}(t) \tag{13}$$

where $\bar{\eta}^m(t) = H(t - m\Delta t)(t - m\Delta t)/\Delta t$ and $H(\cdot)$ indicates the Heaviside step function.

Substituting eq.(12) into eq.(11) yields the discretized boundary integral equation with the unknown coefficients of $[u_i]_q^m$. The discretized equation for the time step of $t = N\Delta t$ may be written in the matrix form as follows:

$$\sum_{m=1}^{N} \left[\quad \boldsymbol{W} \quad \right]^{N-m} \left\{ \quad [\boldsymbol{u}] \quad \right\}^m = - \left\{ \quad \boldsymbol{t}^{in} \quad \right\}^N , \tag{14}$$

or

$$\left[\quad \boldsymbol{W} \quad \right]^0 \left\{ \quad [\boldsymbol{u}] \quad \right\}^N = - \left\{ \quad \boldsymbol{t}^{in} \quad \right\}^N - \sum_{m=1}^{N-1} \left[\quad \boldsymbol{W} \quad \right]^{N-m} \left\{ \quad [\boldsymbol{u}] \quad \right\}^m . \tag{15}$$

Here the components of the matrix $[\boldsymbol{W}]^{N-m}$ are given as

$$[(W_{ij})_{pq}]^{N-m} = p.f. \int_{(m-1)\Delta t}^{(m+1)\Delta t} \int_{S_q} W_{ij}(\boldsymbol{y}, N\Delta t - \tau; \boldsymbol{X}_p)\psi_q(\boldsymbol{y})\eta^m(\tau) dS_y d\tau, \tag{16}$$

where $\boldsymbol{X}_p$ denotes the collocation point on the p-th element. Note that eq.(16), which has integrations over both space and time, can be reduced to the equation involving integration over the spatial domain only, because the time integration can be carried out analytically. Eq.(15) can be solved for the unknown crack-opening displacement $\{[\boldsymbol{u}]\}^N$ $(N = 1, 2, \ldots)$ using the time stepping algorithm.

A difficulty in constructing eq.(15) is to evaluate the hypersingular integrals, which are included in $[\boldsymbol{W}]^0$ on the L.H.S. in eq.(15). The singular component of the matrix $[\boldsymbol{W}]^0$ in the vicinity of the point $\boldsymbol{y} = \boldsymbol{X}_p$ may be reduced to the following form

$$[(W_{ij})_{pp}]^0 = p.f. \int_{S_p} W_{ij}^{st}(\boldsymbol{y}, \boldsymbol{X}_p)\psi_p(\boldsymbol{y}) dS_y + \text{ (regular terms)} , \tag{17}$$

where $\boldsymbol{W}^{st}$ denotes the hypersingular kernel in elastostatics of $O(1/r^3)$. As seen in eq.(17), the singular integrals in elastodynamics can be evaluated in the same way as in elastostatics. There are several regularized methods for evaluating hypersingular integrals. Here we use the subtraction method of higher order as shown in the following equation.

$$\begin{aligned} p.f. \int_{S_p} W_{ik}^{st}(\boldsymbol{y}, \boldsymbol{X}_p)\psi_q(\boldsymbol{y}) dS_y = & \int \Bigg\{ W_{ik}^{st}(\boldsymbol{y}(\boldsymbol{\xi}), \boldsymbol{X}_p)\psi_q(\boldsymbol{y}(\boldsymbol{\xi}))J(\boldsymbol{\xi})\Big|_{y\in S} \\ & - W_{ik}^{st}(\boldsymbol{y}(\boldsymbol{\xi}), \boldsymbol{X}_p) \left[\psi_q(\boldsymbol{X}_p) + (\boldsymbol{y}(\boldsymbol{\xi}) - \boldsymbol{X}_p) \cdot \frac{\partial \psi_q}{\partial \boldsymbol{x}}\Big|_{x=X_p} \right] J'(\boldsymbol{\xi})\Big|_{y\in S'(X_p)} \Bigg\} d\boldsymbol{\xi} \\ & + \psi_q(\boldsymbol{X}_p) p.f. \int_{S'(X_p)} W_{ik}^{st}(\boldsymbol{y}, \boldsymbol{X}_p) dS_y \\ & + \frac{\partial \psi_q}{\partial \boldsymbol{x}}\Big|_{x=X_p} p.v. \int_{S'(X_p)} \cdot(\boldsymbol{y} - \boldsymbol{X}_p) W_{ik}^{st}(\boldsymbol{y}, \boldsymbol{X}_p) dS_y, \end{aligned} \tag{18}$$

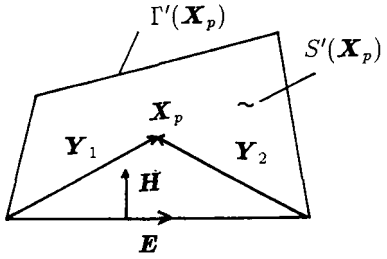

Figure 1: Vectors defined on the plane $S'(\boldsymbol{X}_p)$.

where $S'(\boldsymbol{X}_p)$ is the tangential plane at the point $\boldsymbol{X}_p$, $\boldsymbol{\xi}$ are local coordinates, and $J(\boldsymbol{\xi})$ and $J'(\boldsymbol{\xi})$ are Jacobians. The first integral on the R.H.S. in eq.(18) can be calculated numerically, and the second and the third integrals are evaluated analytically. For example, $p.f.\int_{S'(X_p)} 1/r^3 dS_y$, which is a component of the second integral on the R.H.S. in eq.(18), can be evaluated as follows:

$$\begin{aligned} p.f.\int_{S'(X_p)} 1/r^3 dS_y &= p.f.\int_{S'(X_p)} \frac{\partial}{\partial y_\alpha}\left(-\frac{1}{r^2}\frac{\partial r}{\partial y_\alpha}\right) dS_y \\ &= H_\alpha \int_{\Gamma'(X_p)} \frac{1}{r^2}\frac{\partial r}{\partial y_\alpha} ds_y \\ &= \sum \frac{1}{(\boldsymbol{Y}_1\cdot\boldsymbol{H})}\left(\frac{(\boldsymbol{Y}_2\cdot\boldsymbol{E})}{|\boldsymbol{Y}_2|} - \frac{(\boldsymbol{Y}_1\cdot\boldsymbol{E})}{|\boldsymbol{Y}_1|}\right), \end{aligned} \tag{19}$$

where $\Gamma'(\boldsymbol{X}_p)$ is a contour of the plane $S'(\boldsymbol{X}_p)$ and $\boldsymbol{Y}_1$, $\boldsymbol{Y}_2$, $\boldsymbol{H}$ and $\boldsymbol{E}$ are vectors defined in Fig. 1. In eq.(19), the summation is taken over all the edges of the plane $S'(\boldsymbol{X}_p)$.

4. SCATTERED FAR-FIELD

In the ultrasonic QNDE, scattered waves are usually observed at a point, which is located far away from a crack. Hence, it is of great importance for the ultrasonic crack detection to investigate the properties of scattered far-fields. On the assumption that the dimension of a crack is relatively small in comparison with the distance between the crack and the observation point, the scattered far-field is obtained by making an approximation of the following form in equation (7):

$$|\boldsymbol{x}-\boldsymbol{\xi}| \approx x - \hat{\boldsymbol{x}}\cdot\boldsymbol{\xi}, \tag{20}$$

where $\hat{\boldsymbol{x}}$ is a unit vector in the direction $\boldsymbol{x}$ and $x = |\boldsymbol{x}|$. Taking account of only the terms of $O(x^{-1})$ in equation (7), the scattered far-field may be written as

$$\begin{aligned} u_k^{sc}(\boldsymbol{x},t) &= \frac{c_T^2}{4\pi x c_L^3}\hat{x}_k\left\{\left(\frac{c_L^2}{c_T^2}-2\right)\delta_{pq} + 2\hat{x}_p\hat{x}_q\right\}\int_S n_q(\boldsymbol{\xi})[\dot{u}_p(\boldsymbol{\xi}, t-\frac{x}{c_L}+\frac{\hat{\boldsymbol{x}}\cdot\boldsymbol{\xi}}{c_L})]dS_\xi \\ &+ \frac{1}{4\pi x c_T}(\delta_{kp}\hat{x}_q + \delta_{kq}\hat{x}_p - 2\hat{x}_k\hat{x}_p\hat{x}_q)\int_S n_q(\boldsymbol{\xi})[\dot{u}_p(\boldsymbol{\xi}, t-\frac{x}{c_T}+\frac{\hat{\boldsymbol{x}}\cdot\boldsymbol{\xi}}{c_T})]dS_\xi. \end{aligned} \tag{21}$$

It is more convenient to express the components in spherical polar coordinates (r,θ,ϕ), instead of the Cartesian coordinates. The components in the directions (r,θ,ϕ), which represent P-, SH- and SV- waves, respectively, may be written as follows;

$$u_r(\boldsymbol{x},t) = \frac{1}{4\pi x}\Omega_r(\hat{\boldsymbol{x}}, t-\frac{x}{c_L}), \tag{22}$$

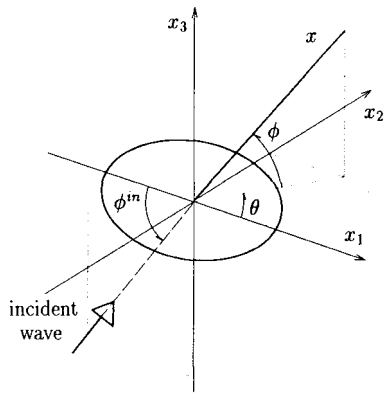

Figure 2: Geometry of the problem.

$$u_\theta(\boldsymbol{x},t) = \frac{1}{4\pi x}\Omega_\theta(\hat{\boldsymbol{x}},t-\frac{x}{c_T}), \tag{23}$$

$$u_\phi(\boldsymbol{x},t) = \frac{1}{4\pi x}\Omega_\phi(\hat{\boldsymbol{x}},t-\frac{x}{c_T}), \tag{24}$$

where

$$\Omega_r(\hat{\boldsymbol{x}},t-\frac{x}{c_L}) = \frac{c_T^2}{c_L^3}\left\{\left(\frac{c_L^2}{c_T^2}-2\right)\delta_{pq}+2\hat{x}_p\hat{x}_q\right\}\int_S n_q(\boldsymbol{\xi})[\dot{u}_p(\boldsymbol{\xi},t-\frac{x}{c_L}+\frac{\hat{\boldsymbol{x}}\cdot\boldsymbol{\xi}}{c_L})]dS_\xi, \tag{25}$$

$$\Omega_\theta(\hat{\boldsymbol{x}},t-\frac{x}{c_T}) = \frac{1}{c_T}(\hat{h}_p\hat{x}_q+\hat{h}_q\hat{x}_p)\int_S n_q(\boldsymbol{\xi})[\dot{u}_p(\boldsymbol{\xi},t-\frac{x}{c_T}+\frac{\hat{\boldsymbol{x}}\cdot\boldsymbol{\xi}}{c_T})]dS_\xi, \tag{26}$$

$$\Omega_\phi(\hat{\boldsymbol{x}},t-\frac{x}{c_T}) = \frac{1}{c_T}(\hat{v}_p\hat{x}_q+\hat{v}_q\hat{x}_p)\int_S n_q(\boldsymbol{\xi})[\dot{u}_p(\boldsymbol{\xi},t-\frac{x}{c_T}+\frac{\hat{\boldsymbol{x}}\cdot\boldsymbol{\xi}}{c_T})]dS_\xi. \tag{27}$$

Here $\hat{\boldsymbol{h}}$ and $\hat{\boldsymbol{v}}$ are unit vectors in the θ and ϕ directions, respectively.

5. NUMERICAL RESULTS

5.1 Statement of the Problem

The geometry of the problem is shown in Fig. 2. A penny-shaped crack is located in the x_1-x_2 plane. The incident wave is either P-, SV-, or SH-plane wave, propagating in the x_1-x_3 plane with the incident angle ϕ^{in}. The displacement of the incident wave is defined by

$$u_i^{in}(\boldsymbol{x},t) = u_0 d_i \frac{p_j x_j - c\,t}{a} H(p_j x_j - c\,t) \tag{28}$$

where u_0 is an amplitude coefficient, a is the radius of the crack. In eq.(28), $\boldsymbol{p}$ is a unit propagation vector given by $\boldsymbol{p} = (\cos\phi^{in}, 0, \sin\phi^{in})$. $\boldsymbol{d}$ and c are a unit vibration vector and a phase velocity, respectively, which are given below, depending the type of the incident wave.

$$\boldsymbol{d} = \begin{cases} (\cos\phi^{in}, 0, \sin\phi^{in}) & \text{for P-wave} \\ (-\sin\phi^{in}, 0, \cos\phi^{in}) & \text{for SV-wave} \\ (0,1,0) & \text{for SH-wave} \end{cases} \tag{29}$$

$$c = \begin{cases} c_L & \text{for P-wave} \\ c_T & \text{for SV-wave} \\ c_T & \text{for SH-wave} \end{cases} \tag{30}$$

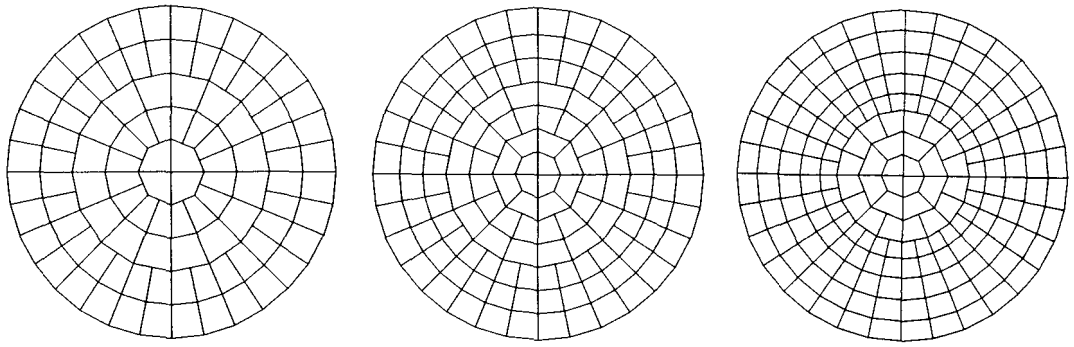

Figure 3: Arrangement of the elements; (a):100 elements, (b):140 elements, (c):188 elements.

The time variation of the incident displacement components is linear as seen in eq.(28), and so the incident stress field shows the time history of a step function. All calculations shown in the sequel are made for Poisson's ratio $\nu = 0.25$.

5.2 Near-Field Solutions

To confirm the accuracy of near-field solutions, we used three types of the arrangement of elements as shown in Fig. 3. 100, 140 and 188 quadrilateral elements are distributed on the crack face as shown in Figs. 3 (a) to (c), respectively. The time increment was chosen as $c_T\Delta t/a = 0.18, 0.13$ and 0.14, corresponding to the element patterns shown in Figs. 3 (a) to (c), respectively.

Fig. 4 shows the time variation of the stress intensity factors K_I at the crack edge $\boldsymbol{x} = (-1, 0, 0)$ subjected to incident P waves with the angles $\phi^{in} = 30°, 60°$ and $90°$. The stress intensity factors K_I can be calculated by using the formula

$$K_I(t) = \frac{\mu\sqrt{2\pi}}{4(1-\nu)} \frac{[u_3(\epsilon, t)]}{\sqrt{\epsilon}}, \tag{31}$$

where ϵ is the distance from the crack edge. In Fig. 4, K_I is normalized by the static stress intensity factor K_I^{st} given by

$$K_I^{st} = 2\mu \frac{u_0}{a} \frac{c_L^2}{c_T^2} \sqrt{a/\pi}. \tag{32}$$

Little difference can be seen among the numerical results obtained for the different distributions of elements.

In the limit as $t \to \infty$, when the incident wave has long since passed, the solution should coincide with the static solution corresponding to the presence of the crack in a linear displacement field of the form $u_i = u_0 d_i p_j x_j/a$. Fig. 5 shows $[u_3]$ as a function x_1/a for the dynamic calculation at the time step of $c_T t/a = 100 c_T \Delta t/a$. The incident waves are P waves with the angles $\phi^{in} = 30°, 60°$ and $90°$. Good agreement is again observed among the results for three different element patterns.

Figs. 4 and 5 suggest that the numbers of elements used here are enough to obtain good accuracy. The element arrangement as shown in Fig. 3 (c) and the time increment $c_T\Delta t/a = 0.14$ are used in the following calculation of scattered far-fields.

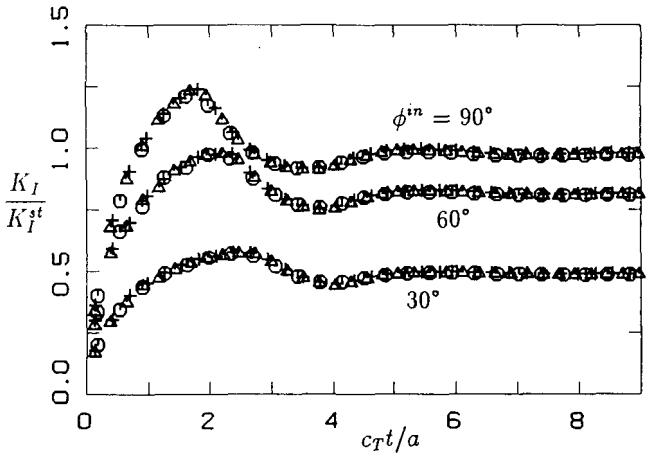

Figure 4: Time variation of the stress intensity factors K_I at the crack edge $\boldsymbol{x} = (-1, 0, 0)$ subjected to incident P waves with the angles $\phi^{in} = 30°, 60°$ and 90°; ○: Fig. 3 (a), △: Fig. 3 (b), +: Fig. 3 (c).

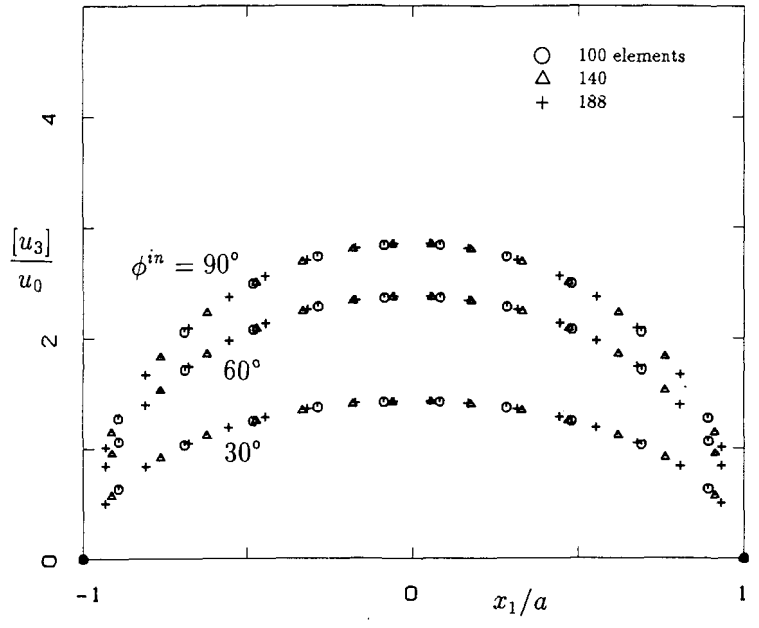

Figure 5: $[u_3]$ as a function x_1/a for the dynamic calculation at the time step of $c_T t/a = 100 c_T \Delta t/a$. The incident waves are P waves with the angles $\phi^{in} = 30°, 60°$ and 90°; ○: Fig. 3 (a), △: Fig. 3 (b), +: Fig. 3 (c).

5.3 Far-Field Solutions

Once the unknown crack-opening displacements have been determined by solving the boundary integral equation (11), the scattered far-fields can be obtained by substituting the crack-opening displacements into eqs.(25) to (27).

Fig. 6 shows the far-field responses Ω_r in the x_1-x_3 plane as a function of time for various values of the angle ϕ. Figs. 6 (a) to (d) correspond to the results for the incident P waves with the incident angles $\phi^{in} = 0°, 30°, 60°$ and $90°$, respectively. As the incident angle ϕ^{in} decreases, the scattered far-fields show smaller amplitudes. The reason is that the effective crack area, which is defined as the crack faces illuminated directly by the incident wave, becomes small as ϕ^{in} decreases. The maximum amplitudes are observed in the forward- and back-scattered waves when the P wave is normally incident to the crack. Here the forward- and back-scattered waves are defined as the scattered waves propagating in the directions $\hat{\boldsymbol{x}} = \boldsymbol{p}$ and $-\boldsymbol{p}$, respectively, where $\boldsymbol{p}$ is a unit propagation vector of the incident wave. For oblique incidences, large amplitudes are found in the forward-scattered and reflected directions. It is also very interesting to see that large amplitudes are generated in the opposite direction to the reflected direction. In the case of $\phi^{in} = 60°$, for example, large amplitudes are generated at $\phi = 60°, \theta = 180°$ as well as $\phi = -60°, \theta = 0°$ (reflected direction) and $\phi = 60°, \theta = 0°$ (forward-scattered direction).

Figs. 7 (a) and (b) show the time variation of the forward- and back-scattered P waves at far-field for the plane P wave excitation, respectively. The incident angles of $\phi^{in} = 0°, 30°, 60°$ and $90°$ are considered. The same results, but for the SV to SV scattering and the SH to SH scattering, are shown in Figs. 8 and 9, respectively. For the P to P scattering as shown in Fig. 7, the peak amplitudes of both forward- and back-scattered waves increase as the incident angle ϕ^{in} increase. This monotonous property may be useful for determining the orientation of the crack in QNDE. The SH to SH wave scattering shows the same tendency as in the P to P case, except that the back-scattered waves have the opposite sign to the forward-scattered waves. For the incident wave with the angle $\phi^{in} = 0°$, there is no response in the SH wave scattering. This feature is not desirable from the point of view of the ultrasonic crack detection. Fig. 8 shows complicated responses in the SV to SV scattering. Forward-scattered waves have almost the same amplitudes, independent of the incident angles except for the normal incidence, but back-scattered amplitudes show a rapid change with the incident angle. The reason for the rapid change of the back-scattered waves is no clear at the present time.

6. CONCLUDING REMARKS

The boundary integral equation was used to solve the scattering problem of obliquely incident waves by a penny-shaped crack. The accuracy of the present method was confirmed by comparing the near-field solutions for different arrangement of elements. Scattered far-fields were calculated for various incident waves, and their usefulness in quantitative non-destructive evaluation was discussed. The results shown here are only a part of scattering data required in the ultrasonic QNDE. Further studies are necessary for various crack geometries and incident waves to construct a useful database for the QNDE.

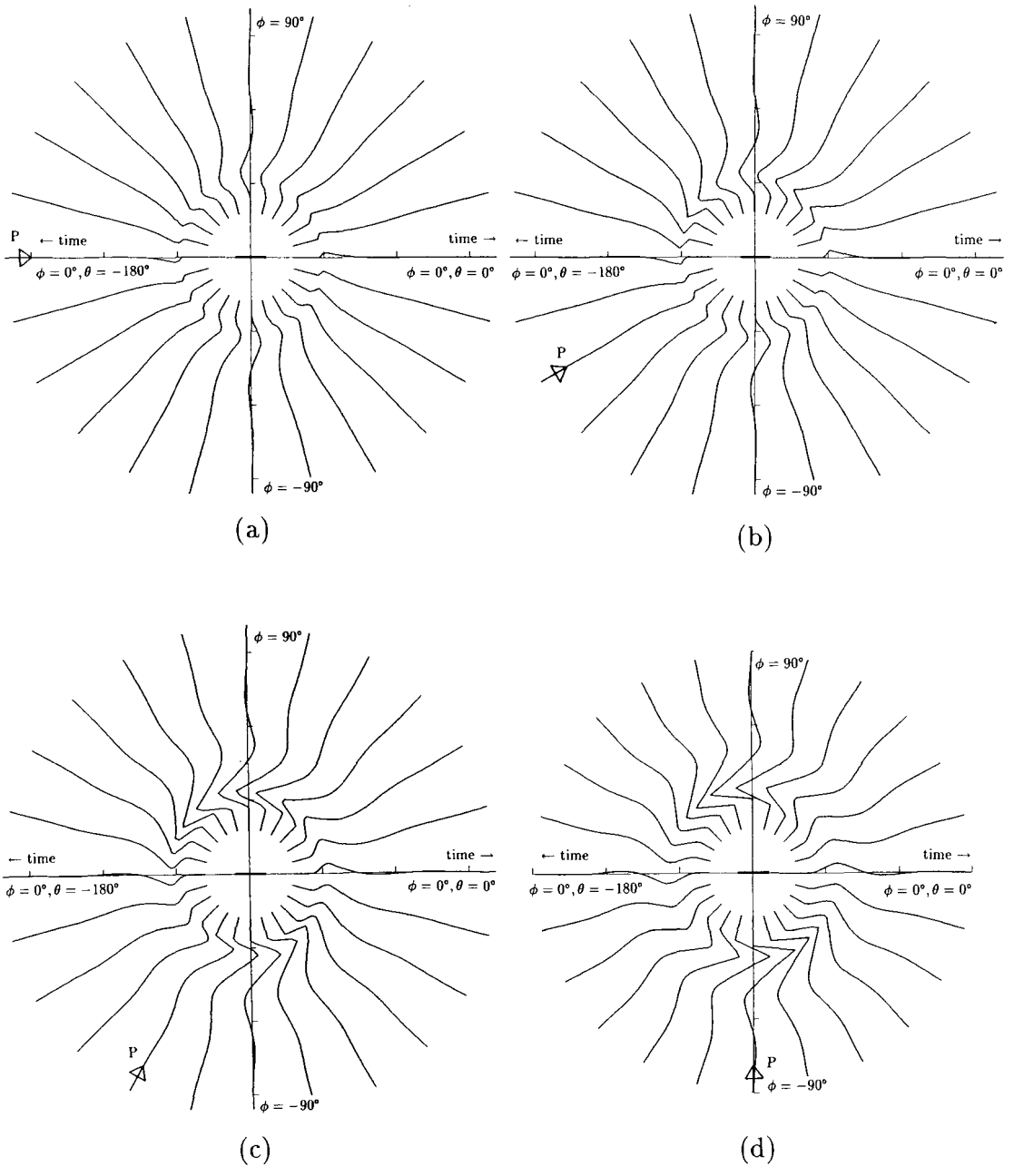

Figure 6: Far-field amplitudes Ω_r in the x_1-x_3 plane as a function of time for the incident P waves with the incident angles ϕ^{in} = (a) 0°, (b) 30°, (c) 60° and (d) 90°.

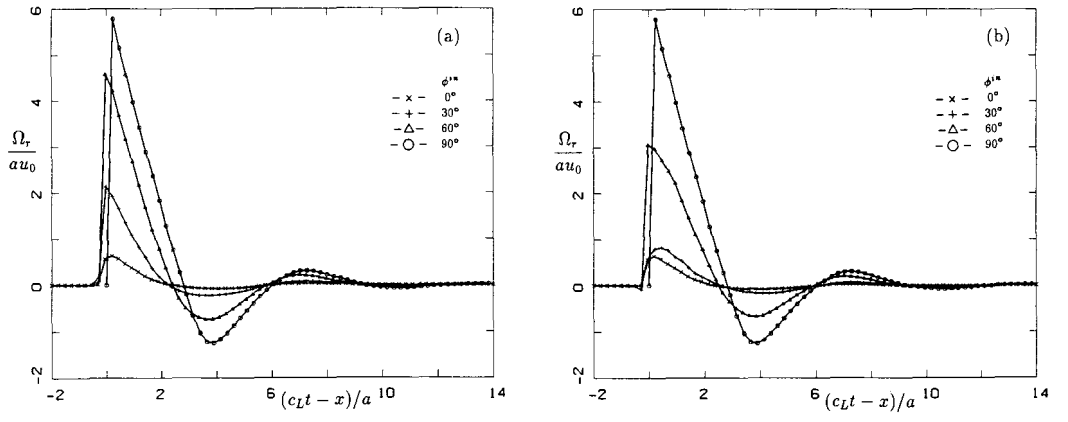

Figure 7: Time variation of the (a) forward- and (b) back-scattered P waves at far-field for the plane P wave excitation. The incident angles of $\phi^{in} = 0°, 30°, 60°$ and $90°$ are considered.

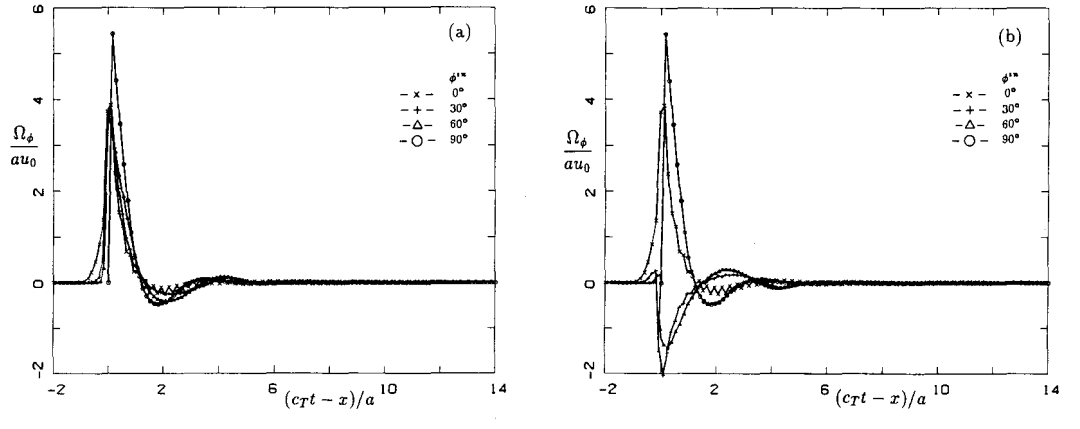

Figure 8: The same as in Fig. 7, but for the SV to SV scattering.

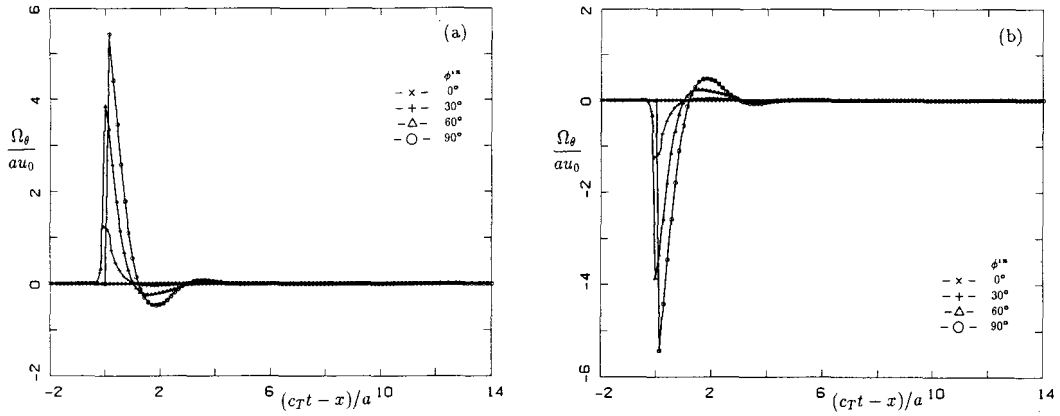

Figure 9: The same as in Fig. 7, but for the SH to SH scattering.

The auther wishes to express his gratitude to Mr. M. Ono of Okayama University for his contribution in the numerical work.

REFERENCES

[1] D. E. Budreck and J. D. Achenbach. Scattering from three-dimensional planar cracks by the boundary integral equation method. *J. Appl. Mech.*, 55, 405–412, 1988.

[2] S. Hirose. Scattering from an elliptic crack by the time-domain boundary integral equation method. In C. A. Brebbia and J. J. Connor, editors, *Advances in Boundary Elements Vol.3 Stress Analysis*, 99–110, Springer, 1989.

[3] S. Hirose and J. D. Achenbach. Application of BEM to transient analysis of a 3-D crack. In M. Tanaka and T. A. Cruse, editors, *Boundary Element Methods in Applied Mechanics*, 255–264, Pergamon Press, Oxford, 1988.

[4] S. Hirose and J. D. Achenbach. Time-domain boundary element analysis of elastic wave interaction with a crack. *Int. J. Numer. Meth. Eng.*, 28, 629–644, 1989.

[5] M. Kitahara, S. Hirose, and J. D. Achenbach. Transient elastodynamic analysis for three-dimensional configurations. In P. K. Banerjee and S. Kobayashi, editors, *Developments in BEM - Vol.7 Advanced Dynamic Analysis Boundary Element Methods*, chapter 7, Elsevier Sci. Pub., Essex, 1992. (in print).

[6] W. Lin and L. M. Keer. Scattering by a planar three-dimensional crack. *J. Acoust. Soc. Am.*, 82(4), 1442–1448, 1987.

[7] P. A. Martin and G. R. Wickham. Diffraction of elastic waves by a penny-shaped crack: analytical and numerical results. *Proc. R. Soc. Lond.*, A 390, 91–129, 1983.

[8] N. Nishimura and S. Kobayashi. A regularized boundary integral equation method for elastodynamic crack problems. *Comput. Mech.*, 4, 319–328, 1989.